AGU ADVANCING EARTH AND SPACE SCIENCE

Geophysical Research Letters®

Key Points:

- Vigorous new particle formation (NPF) above polluted boundary layer was observed over the North China Plain
- Vertical heterogeneities in precursors, oxidizing capacity, and condensation sink favor the NPF in the upper air
- NPF in upper boundary layer has a decisive impact on near-surface aerosol number and cloud condensation nuclei

Author Contributions:

Conceptualization: Xin Huang, Ximeng Qi, Aijun Ding
Formal analysis: Shiyi Lai, Liangduo Chen
Funding acquisition: Xin Huang, Ximeng Qi, Tuukka Petäjä, Markku Kulmala, Aijun Ding
Methodology: Shiyi Lai, Xin Huang, Ximeng Qi, Liangduo Chen, Chuanhua Ren, Zilin Wang, Jinbo Wang, Xuguang Chi, Yang Gao
Resources: Xuguang Chi, Yang Gao, Shangfei Hai
Software: Ximeng Qi, Sijia Lou
Supervision: Xin Huang, Aijun Ding
Validation: Shiyi Lai, Ximeng Qi
Visualization: Shiyi Lai
Writing – original draft: Shiyi Lai, Xin Huang, Ximeng Qi

Vigorous New Particle Formation Above Polluted Boundary Layer in the North China Plain

Shiyi Lai[1,2], Xin Huang[1,2], Ximeng Qi[1,2], Liangduo Chen[1,2], Chuanhua Ren[1,2], Zilin Wang[1,2], Jinbo Wang[1,2], Sijia Lou[1,2], Xuguang Chi[1,2], Yang Gao[3], Shangfei Hai[4], Tuukka Petäjä[5], Veli-Matti Kerminen[5], Markku Kulmala[5], and Aijun Ding[1,2]

[1]School of Atmospheric Sciences, Nanjing University, Nanjing, China, [2]Jiangsu Provincial Collaborative Innovation Center for Climate Change, Nanjing, China, [3]Frontiers Science Center for Deep Ocean Multispheres and Earth System, Key Laboratory of Marine Environment and Ecology, Ministry of Education, Ocean University of China, Qingdao, China, [4]College of Oceanic and Atmospheric Sciences, Ocean University of China, Qingdao, China, [5]Faculty of Science, Institute for Atmospheric and Earth System Research/Physics, University of Helsinki, Helsinki, Finland

Abstract Atmospheric new particle formation (NPF) is vital in climate and air pollution for its contribution to aerosols and cloud condensation nuclei; however, a vertical understanding of NPF is still limited. Here, simultaneous observations at two altitudes were conducted over the North China Plain. Despite a high aerosol loading during cold season, NPF is still frequently observed. The upper-air NPF is increasingly intensive and starts earlier as haze pollution deteriorated, and the onset time gap could exceed 3 hr. To understand the factors modulating NPF vertically, we updated the meteorology-chemistry model by incorporating state-of-the-art nucleation schemes and performed highly vertical-resolved simulations. It is revealed that vertical disparities in NPF are attributed to the pronounced stratification of sulfur dioxide, ozone, and particulate matter. As the evolution of the boundary layer, strong NPF in the upper air elevates the near-surface nucleation-mode particles. This work sheds more light on the vertical structure of NPF.

Plain Language Summary New particle formation (NPF) is a worldwide phenomenon and is regarded as a major contributor to the global cloud condensation nuclei (CCN) as well as to air pollution. Given the vertically varied cloud distribution and the vital role of NPF in CCN, it is of great importance to understand the vertical structure of NPF. However, the overwhelming majority of NPF studies are based on near-surface measurements. By conducting simultaneous observations at two different altitudes in the polluted North China Plain, our study demonstrated that there is an earlier and stronger NPF event in the upper air, especially on polluted days. It is revealed that vertical disparities in NPF are mainly attributed to the pronounced stratification of sulfur dioxide, ozone and particulate matter concentrations in the planetary boundary layer. The differences in NPF onset time together with formation and growth rate in vertical suggest potentially significant impacts on low clouds and particle pollution near the ground. This work shed new light on the vertical structure of NPF and thus their effects on climate change and air pollution.

1. Introduction

New particle formation (NPF), including initial clustering and subsequent growth of these clusters, is frequently observed worldwide (Kerminen et al., 2018; Nieminen et al., 2018; Zhu et al., 2014). It has been recognized that NPF is a major contributor to the global cloud condensation nuclei (CCN) budget as well as to air pollution, thereby posing a substantial impact on climate change and human health (Gordon et al., 2017; Kulmala et al., 2021). Various nucleation mechanisms have been proposed to cause NPF under diverse continental environments, including binary nucleation of H_2SO_4-H_2O (Kulmala et al., 2004; Vehkamäki, 2002), ternary nucleation of H_2SO_4-H_2O involving ammonia and amines (Almeida et al., 2013; Kirkby et al., 2011; Petaja et al., 2011; Yan et al., 2021; Yao et al., 2018), and nucleation of H_2SO_4-H_2O assisted by organic compounds (Metzger et al., 2010; Riccobono et al., 2014; Schobesberger et al., 2013; Zhang et al., 2004). Depending on ambient conditions, especially precursor vapor concentrations, the above nucleation mechanisms may also be assisted by atmospheric ions (Jokinen et al., 2018; Kirkby et al., 2016; Lehtipalo et al., 2018; Yu, 2010). In anthropogenic emission-intensive regions, sulfuric acid (H_2SO_4) has been identified as the main trigger of NPF and amines are likely to be important to stabilize H_2SO_4 cluster (Cai et al., 2022; Huang, Zhou, et al., 2016; Kontkanen et al., 2017; Qi et al., 2018; Sipila et al., 2010; Yan et al., 2021; Yao et al., 2018).

Writing – review & editing: Shiyi Lai, Xin Huang, Ximeng Qi, Sijia Lou, Tuukka Petäjä, Veli-Matti Kerminen, Markku Kulmala, Aijun Ding

Given the vertically varying cloud distribution and the vital role of NPF in the CCN budget, it is of great importance to understand the vertical profile of NPF. As revealed in previous studies, the NPF can be altitude-dependent (Boulon et al., 2011; Lai et al., 2022; Lampilahti et al., 2021; Quan et al., 2017; Zhao et al., 2021). Several aircraft measurement campaigns have been conducted to investigate the vertical distributions of NPF and reported large numbers of small particles at high altitude (Andreae et al., 2018; Krejci et al., 2005; Platis et al., 2016; Takegawa et al., 2020; Wang et al., 2016; Weigel et al., 2011; Williamson et al., 2019; Zhao et al., 2020). Williamson et al. (2019) observed extremely intense NPF activity in the tropical upper troposphere, which is correlated with low temperature and low preexisting aerosol concentration. Wang et al. (2016) and Zhao et al. (2020) showed that high concentrations of small particles formed by organic NPF in the lower free troposphere are transported into the boundary layer in the Amazon. Zhao et al. (2021) demonstrated a preference to observe higher nucleation-mode particle concentrations in the upper mixing layer than at the ground, attributable to the vertical profile of ultraviolet radiation based on measurement at the tower-based platform with a maximum height of 350 m. Using tethered airship, Qi et al. (2019) reported evidence of intensive NPF events above the planetary boundary layer (PBL) of megacities due to high oxidizing capacity, enough condensable vapors, and low condensation sink above the PBL. Boulon et al. (2011) showed that NPF occurred more frequently at the higher elevation due to lower condensation sinks. Based on measurement at the Jungfraujoch station (3,580 m above sea level (a.s.l.)), Bianchi et al. (2016) found that the occurrence of NPF events in the free troposphere was dependent on the availability of precursors transported from the boundary layer.

Observational studies have revealed that NPF-relevant pollutants are nonuniformly distributed in vertical, which is mainly attributed to the PBL evolution. A decreasing $PM_{2.5}$ (particulate matter with aerodynamic diameters less than 2.5 µm) concentrations with an increasing altitude has been wildly observed, with concentrations dropping to 10–20 µg/m^3 near PBL top (Peng et al., 2015; Qi et al., 2019; Wang et al., 2021). It has been acknowledged that low pre-existing aerosol concentrations would favor the occurrence of NPF (Cai et al., 2017; Qi et al., 2019). As an important oxidant, it was reported that the ozone (O_3) concentrations increased sharply above the PBL (Qi et al., 2019; Wang et al., 2021). In addition, previous studies have reported increased concentrations of SO_2—a precursor for NPF—at elevated altitudes (Hong et al., 2021; Huang et al., 2020; Wang et al., 2021). Noteworthily, PBL evolution plays a key role in shaping the chemistry stratification of NPF-relevant pollutants in the PBL by modulating transport process (Huang et al., 2020). It is expected that the PBL evolution processes could greatly modify the stratification of NPF in the boundary layer, in turn, particles formed at NPF-preferential level would influence aerosol number at different altitudes.

Despite being one of the most polluted regions in China, the North China Plain (NCP) has reported a high frequency of NPF events, which further contribute to air pollution as well as CCN (Guo et al., 2014; Kulmala et al., 2021; Ma et al., 2016; Wu et al., 2008). There is a pressing need to quantitatively understand NPF from vertical insights, and this is of paramount importance from the point of view of clouds, especially under such high aerosol loading environment. In this study, by integrating simultaneous measurements at two sites located at the foot and the top of a mountain (160 and 790 m a.s.l.), available air pollutant observations, and model simulations with PBL process diagnosis, we aim to provide a picture of the NPF in the vertical direction over the polluted northern China and understand the impact of PBL dynamics on NPF.

2. Materials and Methods

2.1. Measurement Campaign and Instrumentation

The field campaign on simultaneous measurements at two altitudes was conducted from 3 February to 11 March 2022 in Shijiazhuang (Figure 1a), a representative city suffering from severe pollution in the NCP. During the field campaign, real-time trace gases and aerosol concentrations at the top (790 m a.s.l.) and foot (160 m a.s.l.) of mountain Fenglongshan (114.35°E, 37.92°N), referred to as "Mount FLS Top" and "Mount FLS Foot" respectively (Figure 1b), were simultaneously measured. At the Mount FLS Top site, concentrations of O_3, SO_2, and $PM_{2.5}$ were monitored by a national monitoring station. Aerosol number size distributions were measured continuously with two scanning mobility particle sizers (Nano SMPS and Long SMPS, TSI Inc.) over the size range of 4–1,000 nm. Ceilometer (CL51, Vaisala Inc.) observations were operated at Mount FLS Top, which can provide vertical information on aerosol and cloud. At Mount FLS Foot site, a similar SMPS system (Long SMPS, TSI Inc.) was utilized for measuring the aerosol number size distributions over the size range of 10–1,000 nm. SO_2 concentrations were measured by the trace gas monitor (43i-TLE, ThermoFisher Inc.) at the Mount FLS Foot
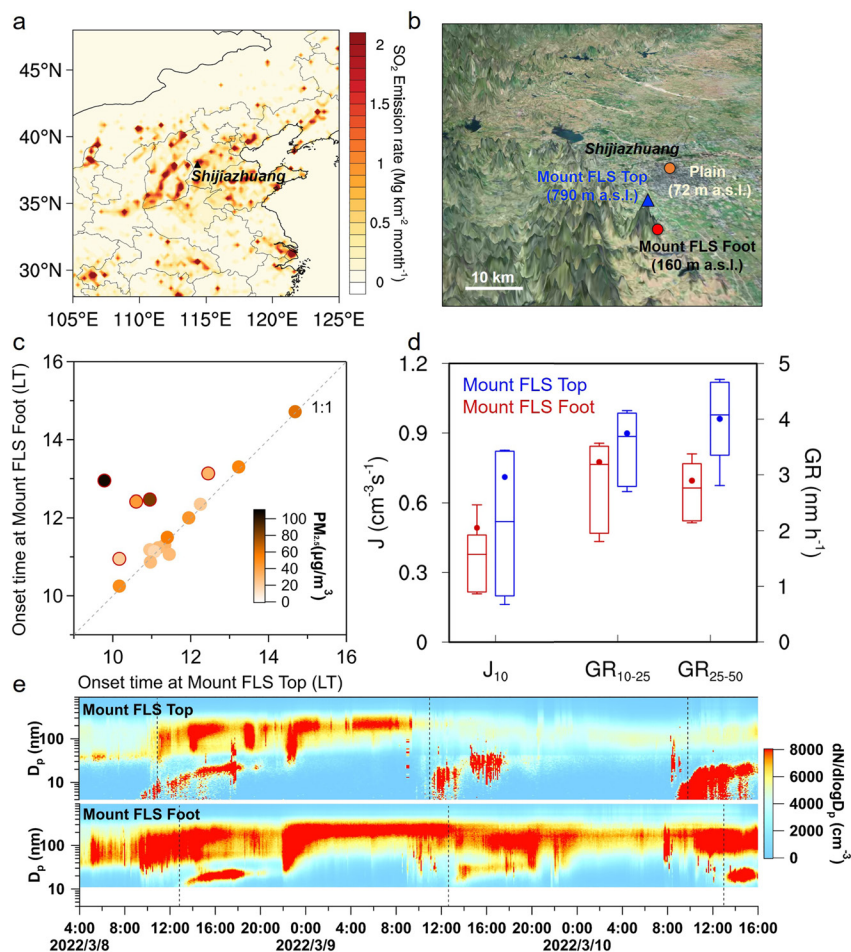
Figure 1. (a) Spatial distributions of SO_2 emission in East China. (b) The locations of observation sites. The blue triangle, red dot, and orange dot mark the Mount FLS Top site, Mount FLS Foot site, and the Plain site, respectively. (c) Comparison of onset times of NPF events between the Mount FLS Top site and Mount FLS Foot site. The points are colored by the $PM_{2.5}$ concentration within PBL (using data at the Plain site). Points with red outlines illustrate the case days with apparent earlier NPF onset time at Mount FLS Top site. LT denotes local time. (d) Box and whisker plot of the formation rate of 10-nm particles (J_{10}), growth rates from 10 to 25 nm (GR_{10-25}), and growth rates from 25 to 50 nm (GR_{25-50}) for the NPF events observed at the Mount FLS Top site and Mount FLS Foot site. The horizontal line in the box represents the median of the data, the dot represents the mean of the data, and the lower and upper edges of the box represent the 25th and 75th percentiles of the data, respectively. The whiskers represent lower to upper tertiles. (e) Comparison of aerosol size distributions at Mount FLS Top site and Mount FLS Foot site from 8 March to 10 March 2022. The vertical dashed line denotes the NPF onset time.

site. To obtain more vertical information on NPF precursors, the air quality measurements at the nearest national monitoring station in the NCP (referred to as "Plain" hereafter, 114.46°E, 38.01°N, 72 m a.s.l., about 13 km northeast to the Mount FLS Foot site; see Figure 1b) were used to investigate the vertical characteristics of SO_2, O_3, and $PM_{2.5}$.

2.2. Improvement of NPF Parameterizations in WRF-Chem

In this study, the Weather Research and Forecasting model coupled with Chemistry (WRF-Chem) model (Grell et al., 2005) version 3.9 with the updated Model for Simulating Aerosol Interaction and Chemistry (MOSAIC) aerosol module (Zaveri et al., 2008) was used. To capture freshly nucleated particles and their growth, the original 4 size bins (covering 39 nm to 10 μm) in the MOSAIC aerosol module were extended to 20 size bins ranging logarithmically from 1 nm to 10 μm (Lai et al., 2022; Lupascu et al., 2015; Matsui et al., 2011). We updated the model by incorporating state-of-the-art nucleation schemes based on laboratory measurements, including binary neutral and ion-induced NPF, ternary neutral and ion-induced (H_2SO_4-NH_3-H_2O) NPF, ternary organic

(H_2SO_4-BioOxOrg-H_2O) NPF as well as H_2SO_4-amine NPF (H_2SO_4-amine-H_2O) (Bergman et al., 2015; Dunne et al., 2016; Gordon et al., 2017). The treatment of NPF parametrizations, BioOxOrg, amine together with uncertainties are detailed in Supporting Information S1 (Text S1 and S2 in Supporting Information S1).

2.3. Simulation Design

To better understand the role of PBL evolution in chemistry stratification and structure of NPF, the one-dimensional WRF-Chem single column model (SCM) with a high vertical resolution was applied, enabling a better representation of PBL evolution (Wang et al., 2018, 2019). The regional dynamic-chemistry coupled modeling was conducted using WRF-Chem model in this study to provide initial concentrations for SCM simulations. The configuration options for regional chemical transport modeling and SCM are described in detail in Supporting Information S1. The SCM simulations were initiated at 04:00 LT (LT: local time) with meteorological input from regional modeling results. The inputted gas and aerosol profiles were extracted from the regional modeling results. Available observations from three measurement sites were assimilated in the initial condition of SO_2 concentration (Figure S2 in Supporting Information S1). To better understand the role of vertical mixing, we conducted parallel numerical experiments with (Vmix-on) and without (Vmix-off) vertical mixing, following the method described in Lai et al. (2022). Furthermore, two simulation scenarios in which nucleation was either on (Nuc-on) or off (Nuc-off) were conducted. To investigate the contributions of PBL vertical mixing to variations of aerosol number concentrations, we performed diagnostic analysis in WRF-Chem modeling (Lai et al., 2022). Although small eddies that may impact local supersaturation are less resolved (Bigg, 1997; Nilsson et al., 2001; Wehner et al., 2010; Wu et al., 2021), given that this study mainly focuses on the influence from daytime NPF stratification, the SCM model is capable of capturing the dominant influence of convective PBL evolution on NPF (Shin & Dudhia, 2016).

3. Results and Discussions

3.1. Distinct Characteristics of NPF at Different Altitudes

A total of 17 NPF events in 37 days occurring at both Mount FLS Top site and Mount FLS Foot site were identified during the campaign based on the criteria suggested by Dal Maso et al. (2005). We defined the onset time of the NPF event as the time when the number concentration of nucleation-mode particles starts to increase from a background concentration. A comparison of the NPF onset times reveals prominent differences between the two different altitude sites, especially when the $PM_{2.5}$ pollution got deteriorated in the lower PBL. As shown in Figure 1c, NPF tended to occur earlier at the higher altitude site on polluted days. To shed more light on the vertical difference of NPF process, here we defined the case day as the day on which NPF starts earlier at Mount FLS Top site compared with Mount FLS Foot site. Accordingly, there are 5 case days on which the onset time is significantly earlier at Mount FLS Top site. Surface $PM_{2.5}$ concentration on the case days was 52% higher than other NPF days, indicating that NPF event that starts earlier at higher altitude is more likely to occur above polluted boundary layer.

Figure 1e presents the temporal variations of particle number size distributions at the two altitude sites during a typical episode (8 March to 10 March 2022) where NPF started earlier at the higher altitude site. During this episode, the averaged $PM_{2.5}$ concentration in the PBL was more than 75 µg m^{-3} (56% higher than the average during the campaign) and NPF occurred earlier at the Mount FLS Top site every morning. NPF event started more than 2 hr earlier at the Mount FLS Top site on average. On the severe pollution day of 10 March (average $PM_{2.5}$ concentration was 106 µg m^{-3}), NPF started earlier at the Mount FLS top site and the onset time difference between the two altitude sites reached 3.1 hr. Particle formation and growth rates (GR) on the typical NPF day were calculated following the procedure described in Kulmala et al. (2012). On these days, the values of formation rates of 10-nm particles (J_{10}) were on average significantly higher at the Mount FLS Top site. The values of GR_{10-25} and GR_{25-50} were comparable between the two sites. As shown, an earlier onset time accompanied with comparable or even higher formation and GR were observed at Mount FLS Top site, indicating that NPF at higher altitude could have a special importance for CCN production.

Figure 1d shows the box-whisker plot of J_{10} and GR at the two sites. The results demonstrate that J_{10} (0.7 cm^{-3} s^{-1}) at the Mount FLS Top site is larger than that observed at the Mount FLS Foot site (0.5 cm^{-3} s^{-1}). Furthermore, the GR, especially in the larger size range (GR_{25-50}) are on average larger at the Mount FLS Top site. The GR_{10-25}
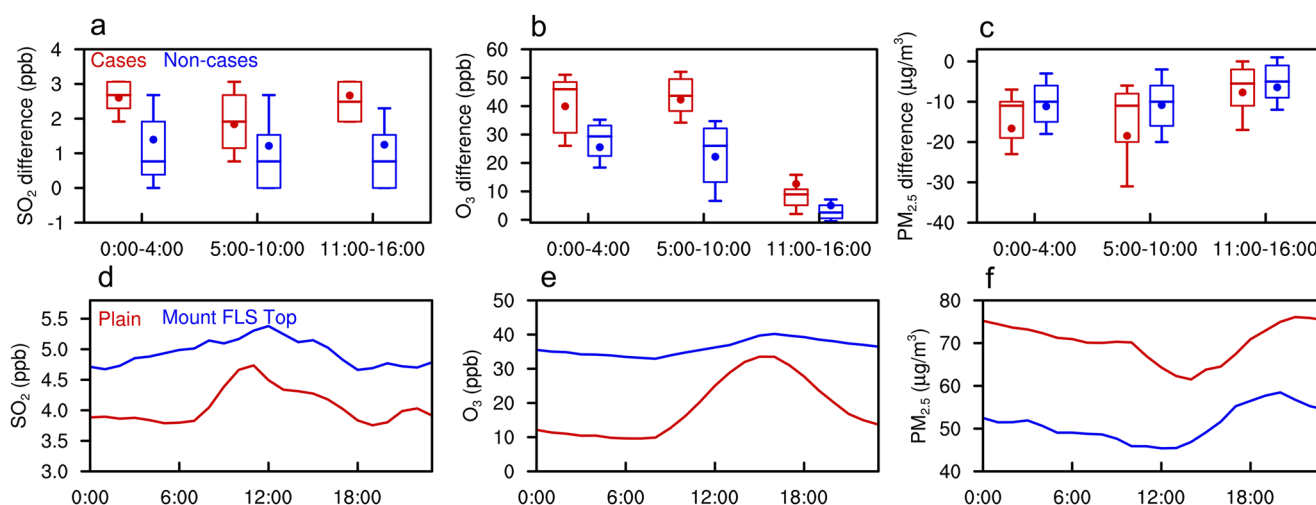
Figure 2. Box and whisker plot of (a) SO_2, (b) O_3, (c) $PM_{2.5}$ difference between Mount FLS Top site and Plain site for case (red) and non-case (blue) days. Diurnal variations of (d) SO_2, (e) O_3, and (f) $PM_{2.5}$ at Mount FLS Top site and Plain site during the cold season (November to April) of 2019–2021.

observed at the Mount FLS Top site were in the range of 2.7–4.2 nm hr^{-1}, with a mean value of 3.7 nm hr^{-1}, being higher than the corresponding values at the Mount FLS Foot site (1.8–3.6 nm hr^{-1} with a mean value of 3.2 nm hr^{-1}). The GR_{25-50} ranged from 2.1 to 3.4 nm hr^{-1} at the Mount FLS Foot site, with an average growth rate of 2.9 nm hr^{-1}, and the corresponding values ranged from 2.8 to 4.7 nm hr^{-1} at the Mount FLS Top site, with an average value of 4.0 nm hr^{-1}. On the case days, the values of J_{10} and GRs were comparable between the two sites (Table S3 in Supporting Information S1), making the onset time a crucial indicator to evaluate the impact of NPF on CCN at high altitudes.

3.2. Steep Gradients of SO_2, O_3, and $PM_{2.5}$ and the Linkage With PBL Evolution

To investigate the vertical structure of the key NPF-relevant pollutants and their possible linkage with the evolution of PBL, simultaneous measurements at the Mount FLS Top site and Plain site were utilized. The characteristics of SO_2, O_3, and $PM_{2.5}$ concentration differences between two altitude sites during the campaign are shown in Figures 2a–2c. SO_2 features relatively higher concentrations at the Mount FLS Top site (Figure 2a). SO_2 is an essential precursor of H_2SO_4 that is proven to be the most important controlling precursor for NPF events (Kulmala et al., 2013). Coal combustion from power plants and industry are the main sources of SO_2 emissions in the NCP (Li et al., 2017). Given the stack heights plus the plume rise height, a countergradient (higher concentration as a function of height) of SO_2 is often observed in this region, where coal-fired power plants are densely distributed (Huang et al., 2020; Liu et al., 2015; Xu et al., 2014).

As an indicator of atmospheric oxidizing capacity, O_3 concentration also exhibits the feature of a obvious countergradient, especially at midnight and early morning (Figure 2b). Since turbulence tends to mix pollutants uniformly in a well-developed convective PBL, O_3 concentrations at the two sites become increasingly comparable in the afternoon. The countergradient of O_3 concentration is mainly due to strong NO titration near the ground and enhanced photochemical production at higher altitudes, constructing a structure of chemical PBL as described by Huang et al. (2020). Also, the accumulated $PM_{2.5}$ near the ground (Figure 2c) attenuates the incident solar radiation, making the near-surface environment unfavorable for photochemical production of O_3 (Bellouin et al., 2020). Both high SO_2 concentration and strong atmospheric oxidizing capacity at high altitudes favor the NPF (Shang et al., 2018).

Typically, high pre-existing particle concentration inhibits the occurrence of NPF events by acting as a sink for both freshly nucleated nanoparticles and condensing vapors (Kerminen et al., 2018; Neitola et al., 2011). $PM_{2.5}$ concentrations at two sites are presented in Figure 2c for both case days and non-case days. In view of the fact that most of the pollutants are emitted near the ground, the $PM_{2.5}$ concentration at the Plain site is higher compared with that at the Mount FLS Top site. Since pollutants disperse relatively little in the vertical because of the limited turbulence, $PM_{2.5}$ shows a large difference between two sites before a well-mixed layer forms. Generally,

SO_2, O_3, and $PM_{2.5}$ show clear stratifications in the PBL. Noteworthy is that the gradients of SO_2, O_3, and $PM_{2.5}$ between two sites are steeper on the case days (Figures 2a–2c). Case days are typically characterized by a high concentration of $PM_{2.5}$ near the ground. High aerosol loadings tend to enhance the stability of the boundary layer, which in turn decreases the boundary layer height and consequently causes further increases in near-surface aerosol concentrations, forming a positive feedback favorable for stratification of pollutants and thereby the altitude-dependent NPF (Huang, Ding, et al., 2016; Petaja et al., 2016). In addition to influencing the NPF onset time, the favorable precursor gases concentration and condensation sink at the high altitude support the aforementioned higher formation rate and growth rate observed at the Mount FLS Top site (Figure S3 in Supporting Information S1).

Long-term measurements at Mount FLS Top site and Plain site during the cold season (November to April) from 2019 to 2021 also confirm the obvious vertical differences in SO_2, O_3, and $PM_{2.5}$ concentrations, especially in the early morning (Figures 2d–2f). In terms of SO_2 and O_3, the averaged concentrations at the Mount FLS Top site during 00:00–10:00 LT are 24% and 205% higher than the corresponding surface observations. On the contrary, the average $PM_{2.5}$ concentrations are 44% lower at the Mount FLS Top site. It is expected that H_2SO_4 formation and thus NPF are facilitated in the upper PBL due to enhanced precursor gases and reduced condensation/coagulation sinks (Kulmala et al., 2013). We thus further analyze the interactions between NPF and chemical PBL evolution with the aid of simulations by WRF-Chem.

3.3. The Vertical Heterogeneity of NPF Processes and the Impacts on CCN

To further investigate the influences of physical and chemical processes on the vertical structure of NPF, a one-dimensional meteorology–chemistry online coupled SCM was applied for all the aforementioned case days. Because of the weak vertical dilution during the nighttime, the air pollutants were clearly stratified, with $PM_{2.5}$ accumulating near the surface and the SO_2-concentrated plume staying in the residual layer (Figure 3a). The concentrations of both O_3 and OH radical near the surface were consumed by freshly-emitted primary pollutants like nitrogen oxides (Figure 3b). Given the higher SO_2 concentration and oxidizing capacity, the production of H_2SO_4, which is a key precursor for NPF, is enhanced above the PBL. Besides, as indicated by $PM_{2.5}$ concentration (Figure 3a), the condensation sink of H_2SO_4, was lower at elevated altitudes. As a result, the averaged H_2SO_4 concentration is 1.6 ppt above the PBL while being lower than 0.8 ppt near the surface (Figure 3c).

Due to higher sources and lower sink indicated by the profile of H_2SO_4 and $PM_{2.5}$, nucleation is initiated above the PBL (Figure 3c). As shown in Figure 3e, the nucleation rate starts to increase at the Mount FLS Foot site with a time lag of nearly 2 hr compared with that at the Mount FLS Top site, which is consistent with observed NPF onset time lag (~1.6 hr). In accordance with earlier studies (Cai et al., 2021; Cai et al., 2022; Yao et al., 2018), we find that H_2SO_4-amine nucleation dominates in the boundary layer. Our simulations indicate that H_2SO_4-amine nucleation is also the dominant nucleation mechanism above PBL (Figure S4 in Supporting Information S1) and temperature effect is minor on the vertical structure of NPF. Accounting for the large uncertainties in amine concentrations, we did sensitive tests on the amine-to-ammonia ratio (i.e., 4.2×10^{-3}, 2.3×10^{-3}, and 1.0×10^{-4}) used in this study (Table S2 in Supporting Information S1). The sensitive tests show that this ratio does not greatly affect the vertical distribution of the total nucleation rate (Figure S5 in Supporting Information S1), with the contribution of H_2SO_4-amine nucleation to the total nucleation rate varying in the range of 75%–99%.

The newly-formed particles can rapidly grow into larger sizes by condensational growth in the upper air. Low aerosol loading above the PBL causes a high survival probability of nanoparticles and low condensation sink for gaseous vapors. Moreover, the growing PBL enables updraft transport of anthropogenic gas vapors emitted near the surface. A higher atmospheric oxidizing capacity enables rapid oxidation of gaseous precursors to produce oxidized vapors with relatively low volatility at high altitudes, which further contribute to the growth of newly formed particles. As a result, CN_{1-10} (CN_{d1-d2}: number concentrations of particles in the size range from d1 to d2 nm) and CN_{10-40} also feature an earlier increase in the upper air (Figures 3d and 3e). Comparing the observed and simulated CN_{10-40} during 10:00–13:00 LT at two sites (Figure 3f), the simulation result reproduced a similar signal as shown in measurements, that is, the CN_{10-40} at the Mount FLS Top site is higher than that at the Mount FLS Foot site, confirmed by the large contrast between two sites.

As the surface is continually heated by incident solar radiation, a residual layer with higher values of CN_{10-40} is entrained into the convective mixed layer and elevates the surface CN_{10-40}, with an estimated contribution of 1,500

Figure 3. (a) Average of simulated vertical distributions of SO_2 concentrations for case days. The gray lines mean the contour of averaged simulated $PM_{2.5}$ for case days (unit: $\mu g\ m^{-3}$)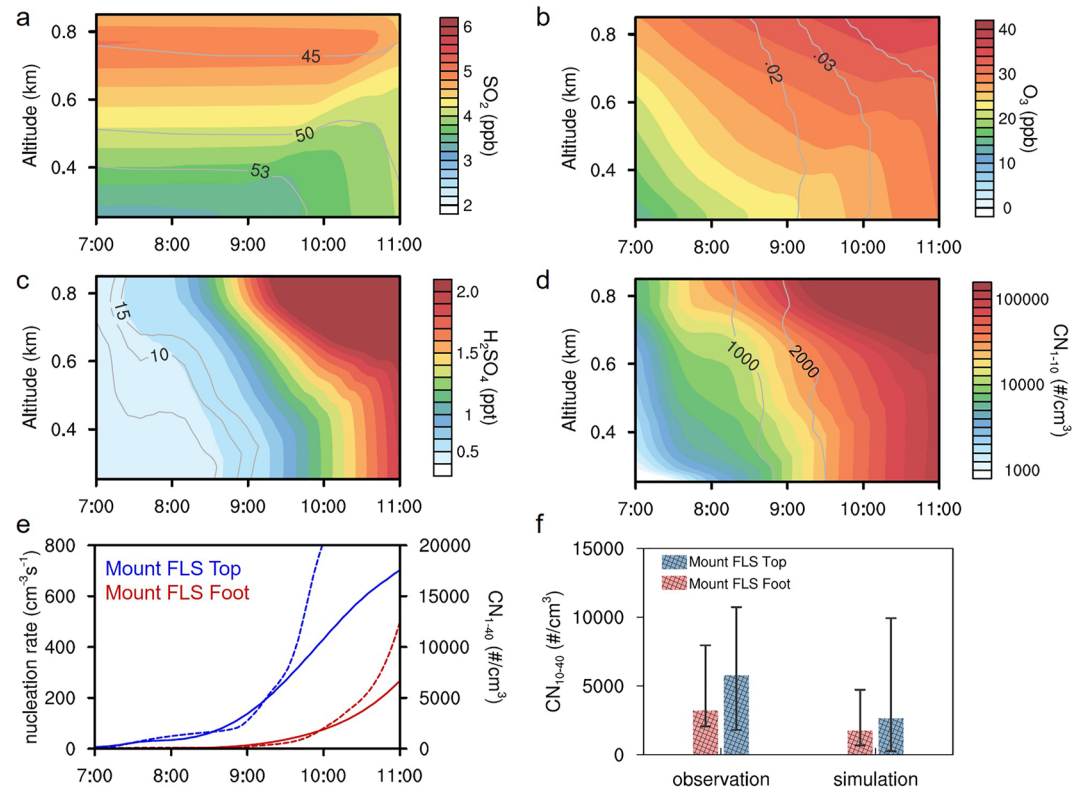. (b) Average of simulated vertical distributions of O_3 concentrations for case days. The gray lines mean the contour of averaged simulated OH radical for case days (unit: ppt). (c) Average of simulated vertical distributions of the sulfuric acid concentration for case days. The gray lines mean the contour of averaged simulated nucleation rate (unit: $cm^{-3}\ s^{-1}$). (d) Average of simulated vertical distributions of the number concentrations of 1–10 nm particles for case days. The gray lines mean the contour of the averaged number concentrations of 10–40 nm particles (unit: $\#\ cm^{-3}$). (e) Average of modeled time series of the nucleation rate (solid lines) and the number concentrations of 1–40 nm particles (dashed lines) at the Mount FLS Top site and Mount FLS Foot site for case days. (f) Observed and modeled number concentrations of 10–40 nm particles at the Mount FLS Top site and Mount FLS Foot site. Note: Bars are the median value during 10:00–13:00 LT on case days. The whiskers represent the 25–75th percentile.

$\#/cm^3$ (51%) of the morning increase (07:00–11:00 LT) (Figure 4a). Comparatively, the overall perturbations of CN_{10-40} caused by PBL mixing (line in Figure 4a) are more substantial than those due to downward transport of nucleation-mode particles from aloft alone (bars in Figure 4a). In the sensitivity test excluding vertical mixing of trace gases and particles, in addition to the suppressed downward transport of nucleation-mode particles aloft, the accumulated $PM_{2.5}$ near the ground cannot be efficiently diluted and the near-surface increment of SO_2 and O_3 due to entrainment is weakened. This thereby indicates that PBL dynamics plays a key role in modifying the vertical profile of NPF, not only by the transport of particles vertically but also by shaping the vertical stratification of NPF-relevant pollutants. Overall, by modifying the vertical structure of CN_{10-40}, precursor gas (SO_2) as well as oxidizing capacity (O_3) and sink (dilution of pre-existing particles), PBL vertical mixing induced an increase of 8,500 $\#/cm^3$ in CN_{10-40} near the surface during 7:00–11:00 LT. A similar phenomenon is confirmed by our previous study (Lai et al., 2022). Due to high Brownian diffusivities, small particles are lost by coagulation scavenging with a low survival probability in the PBL (Kulmala et al., 2017; Wang et al., 2020). Thus, the contribution of vertical transport to CN_{1-10} is minor compared with nucleation (Figure S6 in Supporting Information S1).

The vertical heterogeneity of CN is expected to play a crucial part in CCN availability, especially near the PBL top where the microphysical properties of clouds are quite sensitive to CCN concentrations (Helbig et al., 2021; Huang et al., 2020; Zheng et al., 2021). Noteworthily, shallow cumulus clouds commonly occur atop convective boundary layer and the ceilometer observations did suggest that there generally exists a cloud layer near the PBL top (Figure 4b). The possibility of aerosol being activated as CCN is largely controlled by the particle size at a certain superstation (Dusek et al., 2006; Petters & Kreidenweis, 2007). Particles with diameters greater than
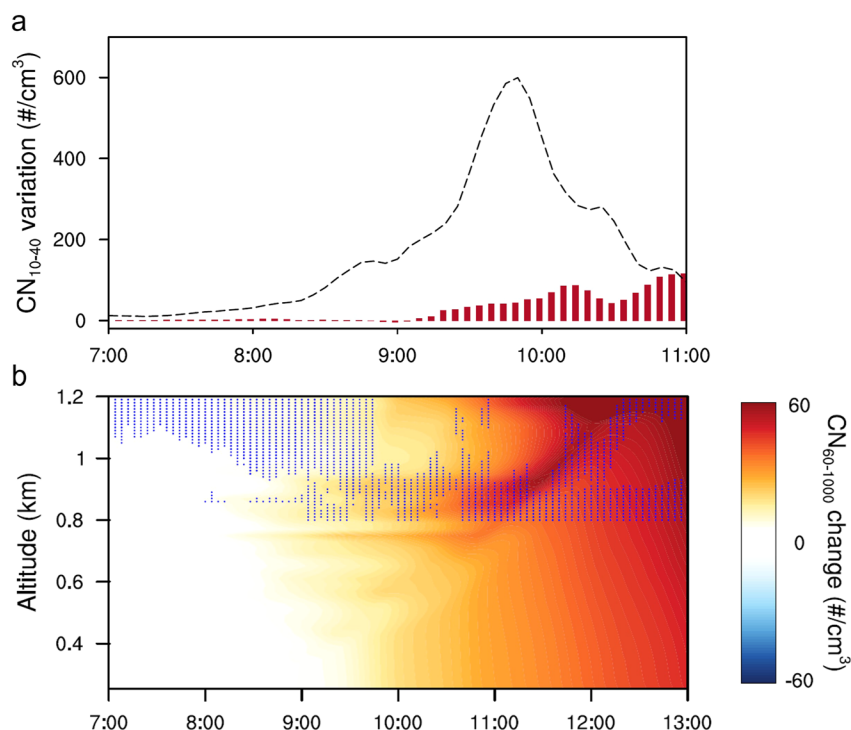
Figure 4. (a) Average the number concentrations of 10–40 nm particles near the ground due to PBL evolution based on WRF-Chem analysis for case days (red bars). Average the influence of vertical mixing on the number concentrations of 10–40 nm particles near the ground for case days (black dashed line). (b) Average nucleation-induced changes in the number concentrations of particles in the size range from 60 to 1,000 nm for case days and cloud identification by ceilometer (blue dots, backscatter greater than 0.01 km^{-1} srad^{-1} during the campaign).

60 nm are large enough to be activated under realistic supersaturation (Williamson et al., 2019). Thus, in this study, we used the $CN_{60-1000}$ as an indicator to show the CCN variation. Given the early onset and high growth rate, NPF leads to a notable enhancement of $CN_{60-1000}$ near the PBL top (an average contribution of 50 #/cm^3 during 10:00–13:00 LT at 800–1,200 m), which could effectively contribute to CCN and modulate the microphysical properties of clouds (Dusek et al., 2006; Spracklen et al., 2008; Williamson et al., 2019).

4. Conclusions

Simultaneous measurements of the particle number size distribution, NPF-relevant gases and aerosol mass concentrations at different altitudes as well as model simulations are combined to understand the vertical stratification of NPF in the highly polluted NCP region. NPF events at higher altitude feature an earlier onset time accompanied by higher formation and growth rate, particularly when haze pollution gets deteriorated, and this onset time gap could exceed 3 hr. The vertical differences in NPF characteristics are mainly attributable to the pronounced stratifications of SO_2, O_3, and $PM_{2.5}$ concentrations. The steeper stratification on highly polluted days contributes to the altitude dependency of NPF. Model simulations predict enhanced CCN concentrations at the PBL top. As the evolution of morning PBL, nucleation-mode particles formed at higher altitudes elevate the concentrations of near-surface nucleation-mode particles, with an estimated contribution of 51% of the morning increase. PBL dynamics not only directly modifies the transport of particles but also shapes the vertical distribution of NPF-relevant pollutants. It induced a larger increase of CN_{10-40} near the surface by modulating the downward transport of nucleation-mode particles, SO_2, and O_3 as well as dilution of pre-existing particles, indicating the important role of PBL dynamics in NPF within PBL. Vigorous NPF accompanied with comparable or even higher formation and GR in the upper air are indicative of the potential importance of vertical NPF stratification in CCN and clouds. This work sheds new light on the vertical structure of NPF in polluted environments and highlights the significance of NPF observation at different altitudes, which is important for improving the understanding of the NPF and its role in air pollution and climate change.

Conflict of Interest

The authors declare no conflicts of interest relevant to this study.

Data Availability Statement

The SO$_2$, O$_3$, and PM$_{2.5}$ mass concentrations and particle number size distribution observations can be downloaded at https://doi.org/10.6084/m9.figshare.20059109.v2. The gridded SO$_2$ monthly emissions for China are available at http://meicmodel.org/?page_id=541&lang=en. The surface weather data are accessible at the Integrated Surface Database (https://www.ncei.noaa.gov/products/land-based-station/integrated-surface-database).

References

Almeida, J., Schobesberger, S., Kurten, A., Ortega, I. K., Kupiainen-Maatta, O., Praplan, A. P., et al. (2013). Molecular understanding of sulphuric acid-amine particle nucleation in the atmosphere. *Nature*, *502*(7471), 359–363. https://doi.org/10.1038/nature12663

Andreae, M. O., Afchine, A., Albrecht, R., Holanda, B. A., Artaxo, P., Barbosa, H. M. J., et al. (2018). Aerosol characteristics and particle production in the upper troposphere over the Amazon Basin. *Atmospheric Chemistry and Physics*, *18*(2), 921–961. https://doi.org/10.5194/acp-18-921-2018

Bellouin, N., Quaas, J., Gryspeerdt, E., Kinne, S., Stier, P., Watson-Parris, D., et al. (2020). Bounding global aerosol radiative forcing of climate change. *Reviews of Geophysics*, *58*(1), e2019RG000660. https://doi.org/10.1029/2019RG000660

Bergman, T., Laaksonen, A., Korhonen, H., Malila, J., Dunne, E. M., Mielonen, T., et al. (2015). Geographical and diurnal features of amine-enhanced boundary layer nucleation. *J. Geophys. Res.-Atmos.*, *120*(18), 9606–9624. https://doi.org/10.1002/2015jd023181

Bianchi, F., Trostl, J., Junninen, H., Frege, C., Henne, S., Hoyle, C. R., et al. (2016). New particle formation in the free troposphere: A question of chemistry and timing. *Science*, *352*(6289), 1109–1112. https://doi.org/10.1126/science.aad5456

Bigg, E. K. (1997). A mechanism for the formation of new particles in the atmosphere. *Atmospheric Research*, *43*(2), 129–137. https://doi.org/10.1016/s0169-8095(96)00020-8

Boulon, J., Sellegri, K., Hervo, M., Picard, D., Pichon, J. M., Fréville, P., & Laj, P. (2011). Investigation of nucleation events vertical extent: A long term study at two different altitude sites. *Atmospheric Chemistry and Physics*, *11*(12), 5625–5639. https://doi.org/10.5194/acp-11-5625-2011

Cai, R. L., Yan, C., Yang, D. S., Yin, R. J., Lu, Y. Q., Deng, C. J., et al. (2021). Sulfuric acid-amine nucleation in urban Beijing. *Atmospheric Chemistry and Physics*, *21*(4), 2457–2468. https://doi.org/10.5194/acp-21-2457-2021

Cai, R. L., Yang, D. S., Fu, Y. Y., Wang, X., Li, X. X., Ma, Y., et al. (2017). Aerosol surface area concentration: A governing factor in new particle formation in Beijing. *Atmospheric Chemistry and Physics*, *17*(20), 12327–12340. https://doi.org/10.5194/acp-17-12327-2017

Cai, R. L., Yin, R. J., Yan, C., Yang, D. S., Deng, C. J., Dada, L., et al. (2022). The missing base molecules in atmospheric acid-base nucleation. *National Science Review*, *13*(10). https://doi.org/10.1093/nsr/nwac137

Dal Maso, M., Kulmala, M., Riipinen, I., Wagner, R., Hussein, T., Aalto, P. P., et al. (2005). Formation and growth of fresh atmospheric aerosols: Eight years of aerosol size distribution data from SMEAR II, Hyytiala, Finland. *Boreal Environment Research*, *10*(5), 323–336.

Dunne, E. M., Gordon, H., Kurten, A., Almeida, J., Duplissy, J., Williamson, C., et al. (2016). Global atmospheric particle formation from CERN CLOUD measurements. *Science*, *354*(6316), 1119–1124. https://doi.org/10.1126/science.aaf2649

Dusek, U., Frank, G. P., Hildebrandt, L., Curtius, J., Schneider, J., Walter, S., et al. (2006). Size matters more than chemistry for cloud-nucleating ability of aerosol particles. *Science*, *312*(5778), 1375–1378. https://doi.org/10.1126/science.1125261

Gordon, H., Kirkby, J., Baltensperger, U., Bianchi, F., Breitenlechner, M., Curtius, J., et al. (2017). Causes and importance of new particle formation in the present-day and preindustrial atmospheres. *J. Geophys. Res.-Atmos.*, *122*(16), 8739–8760. https://doi.org/10.1002/2017jd026844

Grell, G. A., Peckham, S. E., Schmitz, R., McKeen, S. A., Frost, G., Skamarock, W. C., & Eder, B. (2005). Fully coupled "online" chemistry within the WRF model. *Atmospheric Environment*, *39*(37), 6957–6975. https://doi.org/10.1016/j.atmosenv.2005.04.027

Guo, S., Hu, M., Zamora, M. L., Peng, J. F., Shang, D. J., Zheng, J., et al. (2014). Elucidating severe urban haze formation in China. *Proceedings of the National Academy of Sciences of the United States of America*, *111*(49), 17373–17378. https://doi.org/10.1073/pnas.1419604111

Helbig, M., Gerken, T., Beamesderfer, E. R., Baldocchi, D. D., Banerjee, T., Biraud, S. C., et al. (2021). Integrating continuous atmospheric boundary layer and tower-based flux measurements to advance understanding of land-atmosphere interactions. *Agricultural and Forest Meteorology*, *307*, 108509. https://doi.org/10.1016/j.agrformet.2021.108509

Hong, Q. Q., Liu, C., Hu, Q. H., Xing, C. Z., Tan, W., Liu, T., & Liu, J. (2021). Vertical distributions of tropospheric SO$_2$ based on MAX-DOAS observations: Investigating the impacts of regional transport at different heights in the boundary layer. *Journal of Environmental Sciences*, *103*, 119–134. https://doi.org/10.1016/j.jes.2020.09.036

Huang, X., Ding, A. J., Liu, L. X., Liu, Q., Ding, K., Niu, X. R., et al. (2016). Effects of aerosol-radiation interaction on precipitation during biomass-burning season in East China. *Atmospheric Chemistry and Physics*, *16*(15), 10063–10082. https://doi.org/10.5194/acp-16-10063-2016

Huang, X., Huang, J. T., Ren, C. H., Wang, J. P., Wang, H. Y., Wang, J. D., et al. (2020). Chemical boundary layer and its impact on air pollution in northern China. *Environmental Science & Technology Letters*, *7*(11), 826–832. https://doi.org/10.1021/acs.estlett.0c00755

Huang, X., Zhou, L. X., Ding, A. J., Qi, X. M., Nie, W., Wang, M. H., et al. (2016). Comprehensive modelling study on observed new particle formation at the SORPES station in Nanjing, China. *Atmospheric Chemistry and Physics*, *16*(4), 2477–2492. https://doi.org/10.5194/acp-16-2477-2016

Jokinen, T., Sipila, M., Kontkanen, J., Vakkari, V., Tisler, P., Duplissy, E. M., et al. (2018). Ion-induced sulfuric acid-ammonia nucleation drives particle formation in coastal Antarctica. *Science Advances*, *4*(11), 6. https://doi.org/10.1126/sciadv.aat9744

Kerminen, V. M., Chen, X. M., Vakkari, V., Petaja, T., Kulmala, M., & Bianchi, F. (2018). Atmospheric new particle formation and growth: Review of field observations. *Environmental Research Letters*, *13*(10), 38. https://doi.org/10.1088/1748-9326/aadf3c

Kirkby, J., Curtius, J., Almeida, J., Dunne, E., Duplissy, J., Ehrhart, S., et al. (2011). Role of sulphuric acid, ammonia and galactic cosmic rays in atmospheric aerosol nucleation. *Nature*, *476*(7361), 429–433. https://doi.org/10.1038/nature10343

Kirkby, J., Duplissy, J., Sengupta, K., Frege, C., Gordon, H., Williamson, C., et al. (2016). Ion-induced nucleation of pure biogenic particles. *Nature*, *533*(7604), 521–526. https://doi.org/10.1038/nature17953

Kontkanen, J., Lehtipalo, K., Ahonen, L., Kangasluoma, J., Manninen, H. E., Hakala, J., et al. (2017). Measurements of sub-3 nm particles using a particle size magnifier in different environments: From clean mountain top to polluted megacities. *Atmospheric Chemistry and Physics*, *17*(3), 2163–2187. https://doi.org/10.5194/acp-17-2163-2017

Krejci, R., Strom, J., de Reus, M., Williams, J., Fischer, H., Andreae, M. O., & Hansson, H. C. (2005). Spatial and temporal distribution of atmospheric aerosols in the lowermost troposphere over the Amazonian tropical rainforest. *Atmospheric Chemistry and Physics*, *5*(6), 1527–1543. https://doi.org/10.5194/acp-5-1527-2005

Kulmala, M., Dada, L., Daellenbach, K. R., Yan, C., Stolzenburg, D., Kontkanen, J., et al. (2021). Is reducing new particle formation a plausible solution to mitigate particulate air pollution in Beijing and other Chinese megacities? *Faraday Discussions*, *226*, 334–347. https://doi.org/10.1039/d0fd00078g

Kulmala, M., Kerminen, V. M., Petaja, T., Ding, A. J., & Wang, L. (2017). Atmospheric gas-to-particle conversion: Why NPF events are observed in megacities? *Faraday Discussions*, *200*, 271–288. https://doi.org/10.1039/c6fd00257a

Kulmala, M., Kontkanen, J., Junninen, H., Lehtipalo, K., Manninen, H. E., Nieminen, T., et al. (2013). Direct observations of atmospheric aerosol nucleation. *Science*, *339*(6122), 943–946. https://doi.org/10.1126/science.1227385

Kulmala, M., Petaja, T., Nieminen, T., Sipila, M., Manninen, H. E., Lehtipalo, K., et al. (2012). Measurement of the nucleation of atmospheric aerosol particles. *Nature Protocols*, *7*(9), 1651–1667. https://doi.org/10.1038/nprot.2012.091

Kulmala, M., Vehkamaki, H., Petaja, T., Dal Maso, M., Lauri, A., Kerminen, V. M., et al. (2004). formation and growth rates of ultrafine atmospheric particles: A review of observations. *Journal of Aerosol Science*, *35*(2), 143–176. https://doi.org/10.1016/j.jaerosci.2003.10.003

Lai, S. Y., Hai, S. F., Gao, Y., Wang, Y. H., Sheng, L. F., Lupascu, A., et al. (2022). The striking effect of vertical mixing in the planetary boundary layer on new particle formation in the Yangtze River Delta. *Science of the Total Environment*, *829*, 11. https://doi.org/10.1016/j.scitotenv.2022.154607

Lampilahti, J., Leino, K., Manninen, A., Poutanen, P., Franck, A., Peltola, M., et al. (2021). Aerosol particle formation in the upper residual layer. *Atmospheric Chemistry and Physics*, *21*(10), 7901–7915. https://doi.org/10.5194/acp-21-7901-2021

Lehtipalo, K., Yan, C., Dada, L., Bianchi, F., Xiao, M., Wagner, R., et al. (2018). Multicomponent new particle formation from sulfuric acid, ammonia, and biogenic vapors. *Science Advances*, *4*(12), 9. https://doi.org/10.1126/sciadv.aau5363

Li, M., Zhang, Q., Kurokawa, J., Woo, J. H., He, K. B., Lu, Z. F., et al. (2017). MIX: A mosaic Asian anthropogenic emission inventory under the international collaboration framework of the MICS-Asia and HTAP. *Atmospheric Chemistry and Physics*, *17*(2), 935–963. https://doi.org/10.5194/acp-17-935-2017

Liu, F., Zhang, Q., Tong, D., Zheng, B., Li, M., Huo, H., & He, K. B. (2015). High-resolution inventory of technologies, activities, and emissions of coal-fired power plants in China from 1990 to 2010. *Atmospheric Chemistry and Physics*, *15*(23), 13299–13317. https://doi.org/10.5194/acp-15-13299-2015

Lupascu, A., Easter, R., Zaveri, R., Shrivastava, M., Pekour, M., Tomlinson, J., et al. (2015). Modeling particle nucleation and growth over northern California during the 2010 CARES campaign. *Atmospheric Chemistry and Physics*, *15*(21), 12283–12313. https://doi.org/10.5194/acp-15-12283-2015

Ma, N., Zhao, C. S., Tao, J. C., Wu, Z. J., Kecorius, S., Wang, Z. B., et al. (2016). Variation of CCN activity during new particle formation events in the North China Plain. *Atmospheric Chemistry and Physics*, *16*(13), 8593–8607. https://doi.org/10.5194/acp-16-8593-2016

Matsui, H., Koike, M., Kondo, Y., Takegawa, N., Wiedensohler, A., Fast, J. D., & Zaveri, R. A. (2011). Impact of new particle formation on the concentrations of aerosols and cloud condensation nuclei around Beijing. *Journal of Geophysical Research*, *116*(D19), D19208. https://doi.org/10.1029/2011jd016025

Metzger, A., Verheggen, B., Dommen, J., Duplissy, J., Prevot, A. S., Weingartner, E., et al. (2010). Evidence for the role of organics in aerosol particle formation under atmospheric conditions. *Proceedings of the National Academy of Sciences of the United States of America*, *107*(15), 6646–6651. https://doi.org/10.1073/pnas.0911330107

Neitola, K., Asmi, E., Komppula, M., Hyvärinen, A. P., Raatikainen, T., Panwar, T. S., et al. (2011). New particle formation infrequently observed in Himalayan foothills – Why? *Atmospheric Chemistry and Physics*, *11*(16), 8447–8458. https://doi.org/10.5194/acp-11-8447-2011

Nieminen, T., Kerminen, V. M., Petaja, T., Aalto, P. P., Arshinov, M., Asmi, E., et al. (2018). Global analysis of continental boundary layer new particle formation based on long-term measurements. *Atmospheric Chemistry and Physics*, *18*(19), 14737–14756. https://doi.org/10.5194/acp-18-14737-2018

Nilsson, E. D., Rannik, U., Kulmala, M., Buzorius, G., & O'Dowd, C. D. (2001). Effects of continental boundary layer evolution, convection, turbulence and entrainment, on aerosol formation. *Tellus Series B Chemical and Physical Meteorology*, *53*(4), 441–461. https://doi.org/10.1034/j.1600-0889.2001.530409.x

Peng, Z. R., Wang, D. S., Wang, Z. Y., Gao, Y., & Lu, S. J. (2015). A study of vertical distribution patterns of PM2.5 concentrations based on ambient monitoring with unmanned aerial vehicles: A case in Hangzhou, China. *Atmospheric Environment*, *123*, 357–369. https://doi.org/10.1016/j.atmosenv.2015.10.074

Petaja, T., Jarvi, L., Kerminen, V. M., Ding, A. J., Sun, J. N., Nie, W., et al. (2016). Enhanced air pollution via aerosol-boundary layer feedback in China. *Scientific Reports*, *6*(1), 18998. https://doi.org/10.1038/srep18998

Petaja, T., Sipila, M., Paasonen, P., Nieminen, T., Kurten, T., Ortega, I. K., et al. (2011). Experimental observation of strongly bound dimers of sulfuric acid: Application to nucleation in the atmosphere. *Physical Review Letters*, *106*(22), 4. https://doi.org/10.1103/PhysRevLett.106.228302

Petters, M. D., & Kreidenweis, S. M. (2007). A single parameter representation of hygroscopic growth and cloud condensation nucleus activity. *Atmospheric Chemistry and Physics*, *7*(8), 1961–1971. https://doi.org/10.5194/acp-7-1961-2007

Platis, A., Altstadter, B., Wehner, B., Wildmann, N., Lampert, A., Hermann, M., et al. (2016). An observational case study on the influence of atmospheric boundary-layer dynamics on new particle formation. *Boundary-Layer Meteorology*, *158*(1), 67–92. https://doi.org/10.1007/s10546-015-0084-y

Qi, X. M., Ding, A. J., Nie, W., Chi, X. G., Huang, X., Xu, Z., et al. (2019). Direct measurement of new particle formation based on tethered airship around the top of the planetary boundary layer in eastern China. *Atmospheric Environment*, *209*, 92–101. https://doi.org/10.1016/j.atmosenv.2019.04.024

Qi, X. M., Ding, A. J., Roldin, P., Xu, Z. N., Zhou, P. T., Sarnela, N., et al. (2018). Modelling studies of HOMs and their contributions to new particle formation and growth: Comparison of boreal forest in Finland and a polluted environment in China. *Atmospheric Chemistry and Physics*, *18*(16), 11779–11791. https://doi.org/10.5194/acp-18-11779-2018

Quan, J. N., Liu, Y. A., Liu, Q., Jia, X. C., Li, X., Gao, Y., et al. (2017). Anthropogenic pollution elevates the peak height of new particle formation from planetary boundary layer to lower free troposphere. *Geophysical Research Letters*, *44*(14), 7537–7543. https://doi.org/10.1002/2017gl074553

Riccobono, F., Schobesberger, S., Scott, C. E., Dommen, J., Ortega, I. K., Rondo, L., et al. (2014). Oxidation products of biogenic emissions contribute to nucleation of atmospheric particles. *Science*, *344*(6185), 717–721. https://doi.org/10.1126/science.1243527

Schobesberger, S., Junninen, H., Bianchi, F., Lonn, G., Ehn, M., Lehtipalo, K., et al. (2013). Molecular understanding of atmospheric particle formation from sulfuric acid and large oxidized organic molecules. *Proceedings of the National Academy of Sciences of the United States of America*, *110*(43), 17223–17228. https://doi.org/10.1073/pnas.1306973110

Shang, D., Hu, M., Zheng, J., Qin, Y., Du, Z., Li, M., et al. (2018). Particle number size distribution and new particle formation under the influence of biomass burning at a high altitude background site at Mt. Yulong (3410 m), China. *Atmospheric Chemistry and Physics*, *18*(21), 15687–15703. https://doi.org/10.5194/acp-18-15687-2018

Shin, H. H., & Dudhia, J. (2016). Evaluation of PBL parameterizations in WRF at subkilometer grid spacings: Turbulence statistics in the dry convective boundary layer. *Monthly Weather Review*, *144*(3), 1161–1177. https://doi.org/10.1175/mwr-d-15-0208.1

Sipila, M., Berndt, T., Petaja, T., Brus, D., Vanhanen, J., Stratmann, F., et al. (2010). The role of sulfuric acid in atmospheric nucleation. *Science*, *327*(5970), 1243–1246. https://doi.org/10.1126/science.1180315

Spracklen, D. V., Carslaw, K. S., Kulmala, M., Kerminen, V. M., Sihto, S. L., Riipinen, I., et al. (2008). Contribution of particle formation to global cloud condensation nuclei concentrations. *Geophysical Research Letters*, *35*(6), L06808. https://doi.org/10.1029/2007gl033038

Takegawa, N., Seto, T., Moteki, N., Koike, M., Oshima, N., Adachi, K., et al. (2020). Enhanced new particle formation above the marine boundary layer over the Yellow sea: Potential impacts on cloud condensation nuclei. *J. Geophys. Res.-Atmos.*, *125*(9). https://doi.org/10.1029/2019jd031448

Vehkamäki, H. (2002). An improved parameterization for sulfuric acid–water nucleation rates for tropospheric and stratospheric conditions. *Journal of Geophysical Research*, *107*(D22), 4622. https://doi.org/10.1029/2002jd002184

Wang, D. F., Huo, J. T., Duan, Y. S., Zhang, K., Ding, A. J., Fu, Q. Y., et al. (2021). Vertical distribution and transport of air pollutants during a regional haze event in eastern China: A tethered mega-balloon observation study. *Atmospheric Environment*, *246*, 13. https://doi.org/10.1016/j.atmosenv.2020.118039

Wang, J., Krejci, R., Giangrande, S., Kuang, C., Barbosa, H. M., Brito, J., et al. (2016). Amazon boundary layer aerosol concentration sustained by vertical transport during rainfall. *Nature*, *539*(7629), 416–419. https://doi.org/10.1038/nature19819

Wang, M., Kong, W., Marten, R., He, X. C., Chen, D., Pfeifer, J., et al. (2020). Rapid growth of new atmospheric particles by nitric acid and ammonia condensation. *Nature*, *581*(7807), 184–189. https://doi.org/10.1038/s41586-020-2270-4

Wang, Z. L., Huang, X., & Ding, A. J. (2018). Dome effect of black carbon and its key influencing factors: A one-dimensional modelling study. *Atmospheric Chemistry and Physics*, *18*(4), 2821–2834. https://doi.org/10.5194/acp-18-2821-2018

Wang, Z. L., Huang, X., & Ding, A. J. (2019). Optimization of vertical grid setting for air quality modelling in China considering the effect of aerosol-boundary layer interaction. *Atmospheric Environment*, *210*, 1–13. https://doi.org/10.1016/j.atmosenv.2019.04.042

Wehner, B., Siebert, H., Ansmann, A., Ditas, F., Seifert, P., Stratmann, F., et al. (2010). Observations of turbulence-induced new particle formation in the residual layer. *Atmospheric Chemistry and Physics*, *10*(9), 4319–4330. https://doi.org/10.5194/acp-10-4319-2010

Weigel, R., Borrmann, S., Kazil, J., Minikin, A., Stohl, A., Wilson, J. C., et al. (2011). In situ observations of new particle formation in the tropical upper troposphere: The role of clouds and the nucleation mechanism. *Atmospheric Chemistry and Physics*, *11*(18), 9983–10010. https://doi.org/10.5194/acp-11-9983-2011

Williamson, C. J., Kupc, A., Axisa, D., Bilsback, K. R., Bui, T., Campuzano-Jost, P., et al. (2019). A large source of cloud condensation nuclei from new particle formation in the tropics. *Nature*, *574*(7778), 399–403. https://doi.org/10.1038/s41586-019-1638-9

Wu, H., Li, Z. Q., Li, H. Q., Luo, K., Wang, Y. Y., Yan, P., et al. (2021). The impact of the atmospheric turbulence-development tendency on new particle formation: A common finding on three continents. *National Science Review*, *8*(3), 11. https://doi.org/10.1093/nsr/nwaa157

Wu, Z. J., Hu, M., Lin, P., Liu, S., Wehner, B., & Wiedensohler, A. (2008). Particle number size distribution in the urban atmosphere of Beijing, China. *Atmospheric Environment*, *42*(34), 7967–7980. https://doi.org/10.1016/j.atmosenv.2008.06.022

Xu, W. Y., Zhao, C. S., Ran, L., Lin, W. L., Yan, P., & Xu, X. B. (2014). SO$_2$ noontime-peak phenomenon in the North China Plain. *Atmospheric Chemistry and Physics*, *14*(15), 7757–7768. https://doi.org/10.5194/acp-14-7757-2014

Yan, C., Yin, R. J., Lu, Y. Q., Dada, L. N., Yang, D. S., Fu, Y. Y., et al. (2021). The synergistic role of sulfuric acid, bases, and oxidized organics governing new-particle formation in Beijing. *Geophysical Research Letters*, *48*(7), 12. https://doi.org/10.1029/2020gl091944

Yao, L., Garmash, O., Bianchi, F., Zheng, J., Yan, C., Kontkanen, J., et al. (2018). Atmospheric new particle formation from sulfuric acid and amines in a Chinese megacity. *Science*, *361*(6399), 278–281. https://doi.org/10.1126/science.aao4839

Yu, F. Q. (2010). Ion-mediated nucleation in the atmosphere: Key controlling parameters, implications, and look-up table. *Journal of Geophysical Research*, *115*(D3), D03206. https://doi.org/10.1029/2009jd012630

Zaveri, R. A., Easter, R. C., Fast, J. D., & Peters, L. K. (2008). Model for simulating aerosol interactions and chemistry (MOSAIC). *Journal of Geophysical Research*, *113*(D13), 29. https://doi.org/10.1029/2007jd008782

Zhang, R., Suh, I., Zhao, J., Zhang, D., Fortner, E. C., Tie, X., et al. (2004). Atmospheric new particle formation enhanced by organic acids. *Science*, *304*(5676), 1487–1490. https://doi.org/10.1126/science.1095139

Zhao, B., Shrivastava, M., Donahue, N. M., Gordon, H., Schervish, M., Shilling, J. E., et al. (2020). High concentration of ultrafine particles in the Amazon free troposphere produced by organic new particle formation. *Proceedings of the National Academy of Sciences of the United States of America*, *117*(41), 25344–25351. https://doi.org/10.1073/pnas.2006716117

Zhao, G., Zhu, Y. S., Wu, Z. J., Zong, T. M., Chen, J. C. A., Tan, T. Y., et al. (2021). Impact of aerosol-radiation interaction on new particle formation. *Atmospheric Chemistry and Physics*, *21*(13), 9995–10004. https://doi.org/10.5194/acp-21-9995-2021

Zheng, G. J., Wang, Y., Wood, R., Jensen, M. P., Kuang, C. A., McCoy, I. L., et al. (2021). New particle formation in the remote marine boundary layer. *Nature Communications*, *12*(1), 10. https://doi.org/10.1038/s41467-020-20773-1

Zhu, Y. J., Sabaliauskas, K., Liu, X. H., Meng, H., Gao, H. W., Jeong, C. H., et al. (2014). Comparative analysis of new particle formation events in less and severely polluted urban atmosphere. *Atmospheric Environment*, *98*, 655–664. https://doi.org/10.1016/j.atmosenv.2014.09.043